Journal of Applied Fluid Mechanics, Vol. 11, No. 5, pp. 1153-1162, 2018.
Available online at www.jafmonline.net, ISSN 1735-3572, EISSN 1735-3645.
DOI: 10.29252/jafm.11.05.27857

Design Optimization of Ceiling Fan Blades with Nonlinear Sweep Profile

E. Adeeb[1], C. H. Sohn[1†], A. Maqsood[2] and M. A. Afaq[3]

[1] *School of Mechanical Engineering, Kyungpook National University, Daegu 702-701, South Korea*
[2] *Research Centre for Modeling & Simulation, National University of Sciences and Technology, Islamabad 44000, Islamic Republic of Pakistan*
[3] *Institute of Applied Mathematics, Technical University Dortmund, Dortmund 4427, Germany*

[†]*Corresponding Author Email: chsohn@knu.ac.kr*
(Received April 10, 2017; accepted April 6, 2018)

ABSTRACT

This study pertains to the design optimization of a four-blade ceiling fan to enhance air circulation and energy efficiency. The sweep angle of the blade profile is nonlinear. The design of experiment (DOE) computational fluid dynamics (CFD) and response surface method (RSM) methods were used in parallel to find the optimal design solution. The design variables considered were inboard angle of attack, outboard angle of attack, blade sweep, and tip-chord length. Numerical simulations were conducted using steady state Reynolds-averaged Navier–Stokes (RANS) equations and the Spalart–Allmaras turbulence model. The baseline results were validated through experimental data. Subsequently, the DOE method was employed to generate the blade design which reduce the number of simulations without losing the influence of different geometric parameter interactions. The response variables studied were volume flow rate, mass flow rate, torque, and energy efficiency. The simulations exhibited that flow pattern has a distinct feature and is further classified into three groups. In the end, the optimal blade design was identified using response surface methodology (RSM).

Keywords: Nonlinear sweep; Design of experiments; Blade design; Computational fluid dynamics; Response surface method.

NOMENCLATURE

F	forward sweep
I	inboard angle of attack
O	outboard angle of attack
D	tip width
F_i	external body force
ν	kinematic viscosity
J	control variable
ρ	density of fluid
τ_{ij}	reynolds stress tensor
δ_{ij}	kronecker delta
T_d	decrease in torque
τ	stress tensor
$\boldsymbol{V}$	velocity field
∇	operator
u & v	velocity component
$\bar{u}$	time-averaged velocity component
u'	fluctuating velocity
u'_j	instantaneous velocity component
V_m	increase in volumetric flow rate
M_m	increase in mass flow rate
E_m	increase in energy efficiency

1. INTRODUCTION

Optimal utilization of existing resources is the best way to diminish the gap between demand and supply of energy. Energy-efficient designs of household equipment can reshape urban living. Much effort is currently being directed in this area. Ceiling fans are an essential appliance for tropical countries and are extensively used in the summer season. Two types of fans–axial and centrifugal–are generally used to generate comfort. In axial fans, air enters and leaves the fan with no change in the flow direction, whereas in centrifugal fans, air flow changes its direction twice entering and leaving the fan. Ceiling fans can be characterized as axial fans because there is no change in the direction of air flow. Such types of axial fan designs are driven by high flow rates and low pressure demands.

Schmidt and Patterson (2001) performed a comparative study between conventional ceiling fan blades and newly developed aerodynamic blades. In

their study, they concluded that the new aerodynamic blade designs were vastly more efficient and can save power consumption by up to a factor of three. They also noted that ceiling fans display a humped velocity profile, in which the fan velocity rises near the center of the blade, touches a maximum value, and then starts falling along the blade length at a surface beneath the fan. One of the principal problems with the humped-velocity profile is that, while a very slight air movement is detectable beneath the ceiling fan (hub region), subsequently airflow velocity escalates and reaches a peak value between the blade tip and fan blade center.

Ankuar *et al*. (2004) experimentally investigated the flow field of a ceiling fan with no furnishing in the room. They also tested and explained the humped profile of a ceiling fan blade. Moreover, the flow pattern was characterized into eight different regions. Region 1, immediately beneath the fan, has the greatest flow velocity starting from the center of the blade towards the blade tip; less velocity is detected at the center of the fan (beneath hub area). Air is flowing upwards in Region 2 (wall and floor area) and mixes with air in Region 3 (ceiling area) where it becomes dense. Region 4 is between 1 and 2 and has a velocity magnitude in the order of less than 0.1 m/s. Flow reversal is observed in this region and in Region 2. All other regions are adjacent to the ceiling fan blade and have different velocity profiles. They also demonstrated that winglets and spikes on the ceiling fan blades improved the overall air flow rate.

Ramadan *et al*. (2011) developed an analytical solution to predict the air flow velocity distribution in the downward fan plane to the floor. They also numerically simulated the ceiling fan model and validated their results with Ankuar. They reported that the local downward air flow velocity distribution can be increased by varying the fan rotation speed and confirmed this from their two correlations.

Parker *et al*. (2000) conducted a detailed numerical investigation and studied the effect of air-foil-shaped blades on air flow. Parker observed that using these blades resulted in a 21% increase in air flow, and fan power consumption was reduced considerably. Son *et al*. (2009) studied the thermal effect on humans by using an air conditioner in conjunction with a ceiling fan in a room. Their studies recommended that thermal comfort depends strongly on the vertical air speed of the fan and, in addition, thermal comfort is exclusively dependent on the location of the inlet diffuser and has little to do with the use of a ceiling fan.

Falahat (2011) studied the effect of the number of blades for linear profiles of ceiling fans, and Adeeb *et al*. (2015) studied the effect of the number of blades for a non-linear profile. Both researchers reported that four blades were the optimum number of blades required. A four-blade ceiling fan provided the maximum energy efficiency and air flow rate. Numerous techniques have been used by Afaq *et al*. (2014), Afaq *et al*. (2017), Adeeb *et al*. (2015), Lin and Hsieh (2014), and Makhoul *et al* (2013). to improve the energy efficiency and air flow rate of ceiling fans.

Until now, investigations have been primarily conducted on the linear profile of ceiling fan blades. This study developed a fundamental understanding of the air flow phenomena for non-linear ceiling fan blades placed inside a closed room. A CFD investigation was carried out to find the effect of four parameters on four-blade ceiling fans. Optimization of the four-blade ceiling fan design was the main goal of this investigation. Optimization was conducted using response surface methodology (RSM). The process include first, identified the experimental parameters, subsequently designed the experiment, and then performed the optimization process. This paper is organized such that section 2 details the geometric description and governing equations employed to study the phenomena. Then, numerical methodology and validation studies are presented. In section 3 details of DOE and a comparative study is analyzed and presented between forward and reverse-sweep blades. In Section 4, three-dimensional simulation results obtained by the DOE technique for different velocity profiles in terms of swirl were discussed. After that, optimization of the fan blade design using RSM by applying constraints on the data set is presented. Finally, conclusion is drawn.

2. METHODOLOGY

2.1 Geometry description

A model of the experimental room is shown in Fig. 1. The CFD model was generated to represent the physical test chamber of experiment. The room floor area was 4.5 m by 4.5 m with a 4-m-high ceiling with no furnishings. The ceiling fan was mounted at a height of 1 m below the centre of the ceiling.

The model ceiling fan is described in Fig. 2. Blades of the four-blade fan were 90° apart from each other. The direction of rotation for the fan blades was clockwise. The section of the blade that bonds

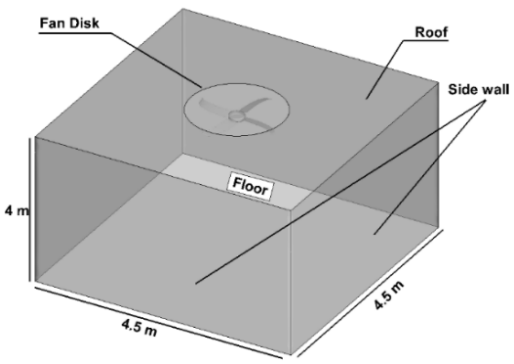

Fig. 1. Ceiling fan room model

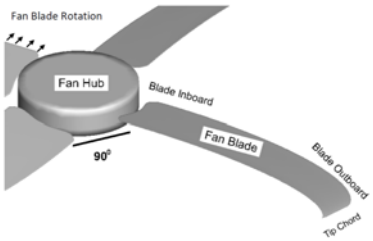

Fig. 2. Ceiling fan description

to the hub is called the inboard section (root), and the other end of the blade is called the outboard section (tip).

2.2 Governing equations

The airflow field modeled in this study was calculated using incompressible Reynolds-averaged Navier–Stokes (RANS) equations. Assuming an incompressible and steady air flow, the continuity and momentum equations were solved using the Moving Reference Frame (MRF) method. The continuity equation for incompressible fluid is defined as

$$\frac{\partial u}{\partial x}+\frac{\partial v}{\partial y}+\frac{\partial w}{\partial z}=0 \tag{1}$$

The momentum equation for incompressible air flows is

$$\frac{\partial(\rho u_i)}{\partial t}+\frac{\partial(\rho u_i u_j)}{\partial x_j}=-\frac{\partial \rho}{\partial x_i}+\frac{\partial \tau_{ij}}{\partial x_j}+\rho g_i + F_i \tag{2}$$

$$\tau_{ij}=\left[\mu\left(\frac{\partial u_i}{\partial x_j}+\frac{\partial u_j}{\partial x_i}\right)\right]-\frac{2}{3}\mu\frac{\partial u_i}{\partial x_i}\delta_{ij} \tag{3}$$

$\tau_{ij}$is the Reynolds stress tensor. The RANS equation can be derived from the Navier–Stokes equation by applying the condition that the velocity component is equal to the sum of the time-averaged velocity component and fluctuating velocity. After solving the Navier–Stokes equation,

$$\frac{\partial(\rho u_i)}{\partial t}+\frac{\partial(\rho u_i u_j)}{\partial x_j}=-\frac{\partial \rho}{\partial x_i}+\frac{\partial \tau_{ij}}{\partial x_j}+\frac{\partial\left(-\rho\overline{u_i' u_j'}\right)}{\partial x_j}+F_x \tag{4}$$

where u_j' is the instantaneous velocity component (i = 1, 2, or 3). The SA turbulence model use one partial differential equation to determine the eddy viscosity.

2.3 Computational modeling

Gambit® software was used to generate the mesh and computational model for the room and the fan. Unstructured tetrahedral mesh elements were used for the meshing room and the fan because they provided flexibility in grid generation. Refined mesh was used to calculate accurate values of the required parameters in computations. The grid was refined in the proximity of the blade surface. A grid-independence study was carried out to improve the accuracy of the model. Afterward turbulence model study was conducted to accurately resolve the velocity magnitude along the walls. A solid wall (no-slip condition) boundary condition was imposed on the room and ceiling fan. A virtual disk contained fan and rotating fluid zone is created. The rest of the computed domain (room volume) was a stationary fluid zone. A connection interface was applied between the fan and the room. An interface boundary condition was applied to separate the rotating and static cell zones. The moving fluid was rotating clockwise with a rotational speed of 300 RPM about the z-axis.

2.4 Validation studies

Before finalizing the grid size, a grid-independence study was carried out using a non-linear ceiling fan blade. To verify the grid influence on the results, three unstructured meshes were generated. A matching grid was made at the interface so there was no discontinuity in flow behavior. Three different room grid sizes (0.7, 1.0, and 1.3 million mesh size) and three fan grid sizes (1.1, 1.3, and 1.6 million mesh size) were used. The grid was chosen on the basis of computational efficiency and maximum flow profile. The final mesh size used for calculations was 0.9 million mesh cells for the room and 1.3 million mesh cells for the fan. The grid independence study showed that a total of two million triangular cells for the room and fan was appropriate to obtain a grid-independent solution. Furthermore, mesh refinement yields insignificant change in the numerical solution. Figure 3 shows the axial velocity of the fan versus the blade inboard-to-outboard distance for the grid-independence study.

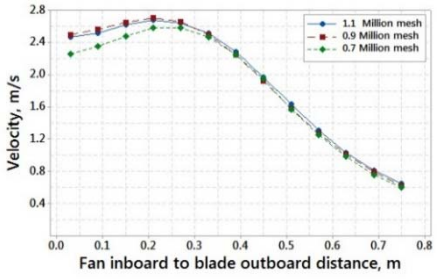

Fig. 3. Grid-independence study for room

The key to the success of CFD lies with an accurate description of the turbulent flow behavior created in a room by a ceiling fan. To model a ceiling fan in a room, a number of turbulence models were studied and result are presented in Fig. 4.

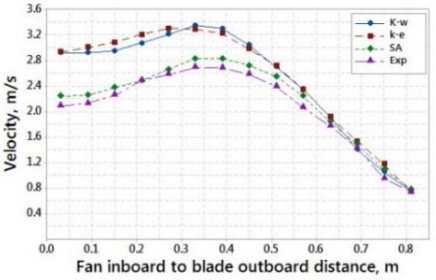

Fig. 4. Experimental and turbulence data validation

To discretize the partial differential equations, the finite volume method was used by applying the SIMPLE algorithm for pressure velocity coupling. To simulate the system, a fixed 300 RPM was specified for the rotating domain and a total pressure of 101325 Pa was used. The second-order discretization scheme was utilized for pressure equation, and the second-order upwind scheme was used for momentum.

3 DESIGN SPACE

In this research, statistical analysis was performed through three main steps: first, a table of design of experiments was constructed with a combination values of the geometrical parameters by giving maximum and minimum values. Second, the runs were performed using the CFD analysis software. Last, the results were gathered and the response surface was obtained. The design variables were sweep (forward or reverse, parametric study conducted on fan undersection), inboard angle of attack (AOA), outboard AOA, and tip chord. The value of inboard and outboard AOA was changed such that the local AOA increased linearly. The response parameters and geometric range of each parameter are presented in Table 1.

3.1 Forward & reverse sweep blade study

A study was carried out on the forward and reverse-sweep blades. For this purpose, two blade designs were selected for a three-blade ceiling fan. Both blades had the same 12° AOA at the inboard and outboard sections, and the tip chord value was 0.117 m. The only design difference between blades 1 and 2 was their sweep value (0.05, 0.15). Blade 2 had a higher sweep value than Blade 1. As shown in Fig. 5, the velocity profile of Blade 1 for forward sweep showed better velocity magnitude near the hub than reverse sweep Blade 1. After covering a distance of 0.4 m, both blades had almost the same velocity magnitude. In the case of Blade 2, which had a high sweep value for forward and reverse sweep (0.15). Near the hub at the first point, the reverse-sweep blade showed minimum magnitude of velocity, but the forward-sweep blade displayed maximum velocity at that point. As moved from the hub outwards, the reverse-sweep blade showed an increase in its velocity magnitude, and its maximum velocity was achieved 0.4 m from the hub and then decreased after that. The forward-sweep blade exhibited an almost constant value of velocity until a distance of 0.25 m from the hub and then decreased sharply until a distance of 0.8 m from the hub.

Regarding the response parameter, the reverse-sweep blade had less volumetric flow rate and mass flow rate compared to the forward-sweep blade (Figs. 6 a & b). In terms of torque (Fig. 6-c), the forward-sweep Blade 1 had greater torque compared to the reverse-sweep Blade 1, but it can be neglected because it had higher energy efficiency (Fig. 6-d) and volumetric flow rate and the difference was minimal. The forward-sweep Blade 2 had less torque and higher energy efficiency compared to reverse-sweep Blade 2. The results revealed that the forward-sweep blade performed better than the reverse-sweep blade. Therefore, all further calculations were conducted with a forward-sweep blade. The volumetric flow rate, mass flow rate, torque, and energy efficiency comparisons are shown in Fig. 6.

Fig. 5. Comparison between forward and reverse sweep blades

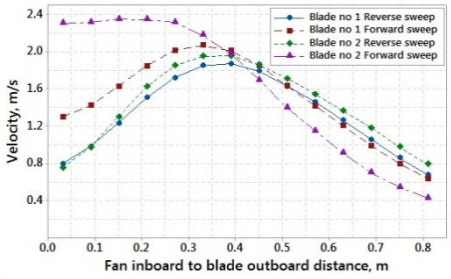

A full factorial 2^k model was used to analyses this problem, and 16 different experiments were created for four-blade ceiling fans. Refer to Table 2 for the design matrix, where '+' represents an upper range of variable and '-' represents a lower range of variable. The first four columns represent the geometric parameters, and the remainder represent geometric parameter interaction. The response of each design is also listed in the table.

4 RESULTS AND DISCUSSION

When a fan is turned on, air starts to revolve randomly and progresses in a downward plane. The interaction between the air flow and the walls produces more complexity in the air flow. This downward diverse velocity is of great significance because it produces dissimilar velocity movement in the room. This phenomenon is explained by Ankuar *et al*. (2004), Schmidt and Patterson (2001) and validated by Bassiouny *et al*. (2011) by performing numerical simulations. Schmidt and Patterson (2001) described the airflow profile as a hump velocity profile, where velocity is in between maximum and minimum values at the inboard section, then reaches its maximum value progressing towards the blade center, after which moving towards the blade outboard section it starts decreasing and reaches its minimum value at a surface beneath the fan.

Based on the contour plots of steady velocity shown in Fig. 7 (surface slice at center of the room x = 0), the following conclusion can be drawn. The velocity contour in the room is composed of two symmetric swirls; the airflow rotates like a solid body (forced vortex), i.e., tangential velocity increases with the radius. In every case, the first vortex had a larger tangential velocity compared to the vortex near the wall. Bassiouny *et al*. (2011) also explained that two symmetric swirl regions are generated about the fan axis, and a separate swirl region is generated near the floor.

Results of this study show that the downward flow patterns had distinct features and can be classified

Table 1 Geometric parameters, range and response parameters

Serial Number	Geometric Parameters with Symbol	Selected Parameters		Response Parameters			
		Low	High				
1	Forward Sweep (F)	0.05 m	0.15 m	Volumetric Flow Rate	Mass Flow Rate	Torque	Energy Efficiency
2	Inboard Angle of Attack (I)	6 deg	12 deg				
3	Outboard Angle of Attack (O)	6 deg	12 deg				
4	Tip Chord (T)	0.058 m	0.117 m				

Table 2. Contrast table and value of response parameters

Deign No	Geometric Parameters				Interactions of Geometric Parameters										Results			
	F	I	O	T	FI	FO	FT	IO	IT	OT	FIO	FIT	FOT	IOT	FIOT	Volumetric Flow Rate (m3/min)	Mass Flow Rate (Kg/m3)	Torque (N.m)	Energy Efficiency (m2/N.min)
1	−	−	−	−	+	+	+	+	+	+	−	−	−	−	+	95.31	1.94	0.72	132.16
2	+	−	−	−	−	−	−	+	+	+	+	+	+	−	−	98.76	2.01	0.79	123.62
3	−	+	−	−	−	+	+	−	−	+	+	+	−	+	−	128.58	2.62	0.98	130.11
4	+	+	−	−	+	−	−	−	−	+	−	−	+	+	+	135.43	2.76	1.09	123.54
5	−	−	+	−	+	−	+	−	+	−	+	−	+	+	−	127.8	2.6	1.29	98.36
6	+	−	+	−	−	+	−	−	+	−	−	+	−	+	+	137.28	2.8	1.55	88.44
7	−	+	+	−	−	−	+	+	−	−	−	+	+	−	+	188.19	3.84	1.83	102.53
8	+	+	+	−	+	+	−	+	−	−	+	−	−	−	−	184.85	3.77	2.13	86.47
9	−	−	−	+	+	+	−	+	−	−	−	+	+	+	−	98.28	2.00	0.8	121.66
10	+	−	−	+	−	−	+	+	−	−	+	−	−	+	+	104.58	2.13	0.875	119.50
11	−	+	−	+	−	+	−	−	+	−	+	−	+	−	+	136.72	2.79	1.09	125.2
12	+	+	−	+	+	−	+	−	+	−	−	+	−	−	−	146.5	2.99	1.19	122.84
13	−	−	+	+	+	−	−	−	−	+	+	+	−	−	+	122.33	2.49	1.45	83.84
14	+	−	+	+	−	+	+	−	−	+	−	−	+	−	−	149.67	3.05	1.72	86.94
15	−	+	+	+	−	−	−	+	+	+	−	−	−	+	−	204.64	4.17	2.08	98.22
16	+	+	+	+	+	+	+	+	+	+	+	+	+	+	+	197.57	4.03	2.26	87.12

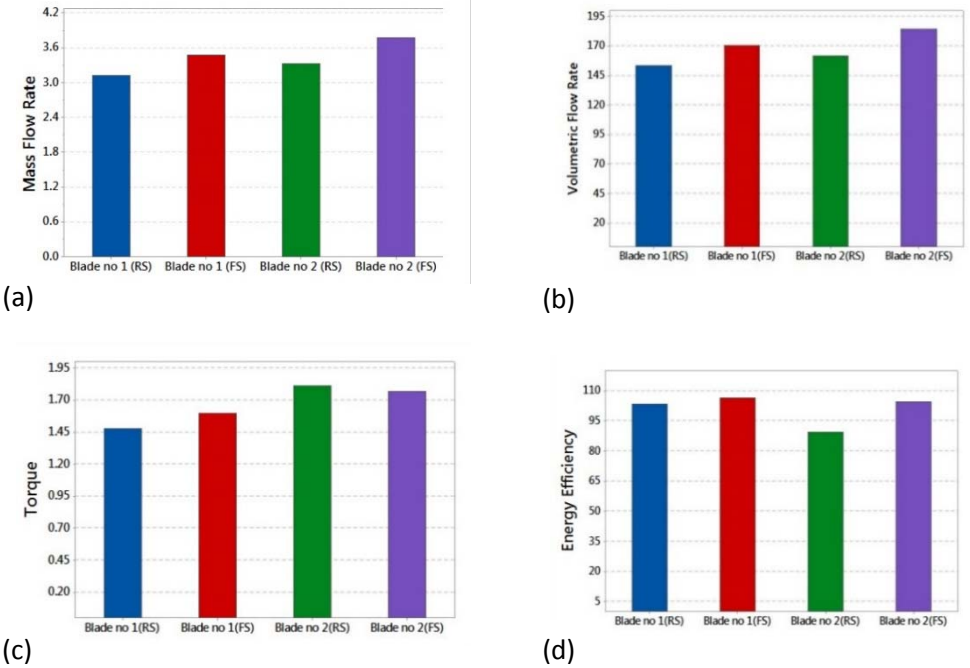

Fig. 6. Comparison of velocity magnitude of, and effect of response parameter on, forward- and reverse-sweep blade designs

into three flow velocity profiles–low-hump velocity, moderate-hump velocity, and high-hump velocity. This classification will facilitate the understanding of the physical behavior of a ceiling fan. This classification is based on a velocity measure near the hub (inboard section, first point) and the difference between the maximum magnitude value between all points.

In the low-hump velocity profile, velocity propagates at approximately 1.45 m/s from the fan axis (near hub) and no further disruption is created as air travels towards the floor. After that, airflow will move along the wall and again re-enter the fan region as explained by Ankuar *et al*. (2004). It is worth mentioning that various swirl patterns were witnessed (Fig. 7). Every fan demonstrated two symmetric swirl regions of different sizes about the fan axis. The low-hump velocity profile, which produces maximum velocity about the fan axis, thrusts the air with greater force towards the floor. The significant phenomena is seen for design numbers 4, 7, 8, 11, 12, 15, and 16. T In the z-direction the swirl region near the blade hub was very small and helped the air to accelerate more in that region. The flow from the fan blade was very powerful which helps to create no swirl region near the floor.

The moderate-hump velocity profile exists when velocity propagates with a value less than 1.45 m/s from the fan axis and the difference between the maximum magnitude value and the hub starting velocity point is less than 0.4 m/s. In this profile, the fan pushes the air towards the floor with less magnitude compared to the low-hump velocity profile, then the air moves along the walls and re-enters the fan region. The order of magnitude near the inboard section was about 1.2 m/s in these simulations. The tangential velocity distribution of the two swirls was approximately symmetric and of the same size (design numbers 1, 2, 9 and 10).

In the high-hump velocity profile (designs 3, 5, 6, 13 and 14), velocity propagates with a value less than 1.45 m/s from the fan axis, and the difference between the maximum magnitude value and the hub starting velocity point is more than 0.4 m/s. An extra strong swirl region was observed near the floor as explained by Bassiouny *et al* (2011).

The stronger the swirl region, the more velocity difference is observed between the maximum magnitude value and the hub starting velocity point. Owing to this swirl region, the nature of the flow is divergent, and the divergence angle depends completely on the strength of the swirl.

Figures 8 and 9 shows the air velocity profile of the sweep ceiling fan blades measured at 1.5 m on the z-axis. Values of velocity magnitude were taken at selected points. The maximum and minimum velocity variations showed the unsteady nature of the ceiling fan flow. Fan blades start losing their effectiveness near the blade tip where velocity decreases effectively. Ankuar *et al*. (2004) mentioned that the last 15–20% of the blade area contributed much less in overall flow rate, which is consistent with our results (blade chord 0.56 m). The velocity profiles that created more thermal comfort were blade designs 7, 8, 15, and 16. The values of the four response parameters selected in this research are listed in Table 2. All values of volumetric flow rate and mass flow rate were taken 1.5 m below the ceiling fan, and measurements were obtained as explained by Adeeb *et al* (2016). In four-blade ceiling fans, the maximum volumetric flow rate and mass flow rate are achieved when inboard and outboard AOA are 12° and minimum when the AOA is 6°. As shown in Table 2, Blade 15 provided the maximum volumetric flow rate and mass flow rate.

Forward sweep shows a moderate effect on volumetric flow rate and mass flow rate. By increasing the non-linearity of a blade's volumetric flow rate and mass flow rate is increased but at the expense of increased torque. By using full tip-width maximum fluid coming downward on a surface 1.5 m below the ceiling fan and by reducing the tip-width volumetric flow rate and mass flow rate decreased, except for Blade 15, which shows a maximum volumetric flow rate and mass flow rate at a low tip-width. This occurred because, at a high AOA, the forward-sweep blade tip-width effect decreases and contributes more to the air flow in the room.

The torque was minimum for Blade 1 when the parameter settings were set at low, and increased as the parameter values increased. The torque increased as we increased the sweep, AOA, and tip width. By using high parametric values, we increased the volumetric flow rate and mass flow rate, but at the expense of torque.

Energy efficiency is a ratio of volumetric flow rate and torque; the higher the torque, the lower is the energy efficiency. Energy efficiency is an important factor, but we cannot singly rely on this parameter. Some designs show greater energy efficiency, but at the same time, these designs are producing a much lower volumetric flow rate and mass flow rate.

4.1 Parmetric analysis

Sensitive analysis of parameter and their interaction provide most sensitive parameter for response parameter. The effect of geometrical parameters and interactions on response parameters are depicted in Fig. 10. Figure 10 (a) indicates the significance of the effect of parameters and interactions on volumetric flow rate. The most influential response parameter was outboard AOA (O), followed by the inboard AOA (I) for volumetric flow rate, mass flow rate (Fig. 10-b), and torque (Fig. 10-c). For energy efficiency (Fig. 10-d), forward sweep (F) was the most important parameter. The most significant interaction combination was consistent with inboard and outboard AOA (IO), followed by forward sweep, outboard AOA and inboard AOA (FIO). The least influential parameter was tip chord (T).

Figure 11 shows the response surface in the three-dimensional space between mass flow rate, energy efficiency, and torque and trade-off between different factors can be observed.

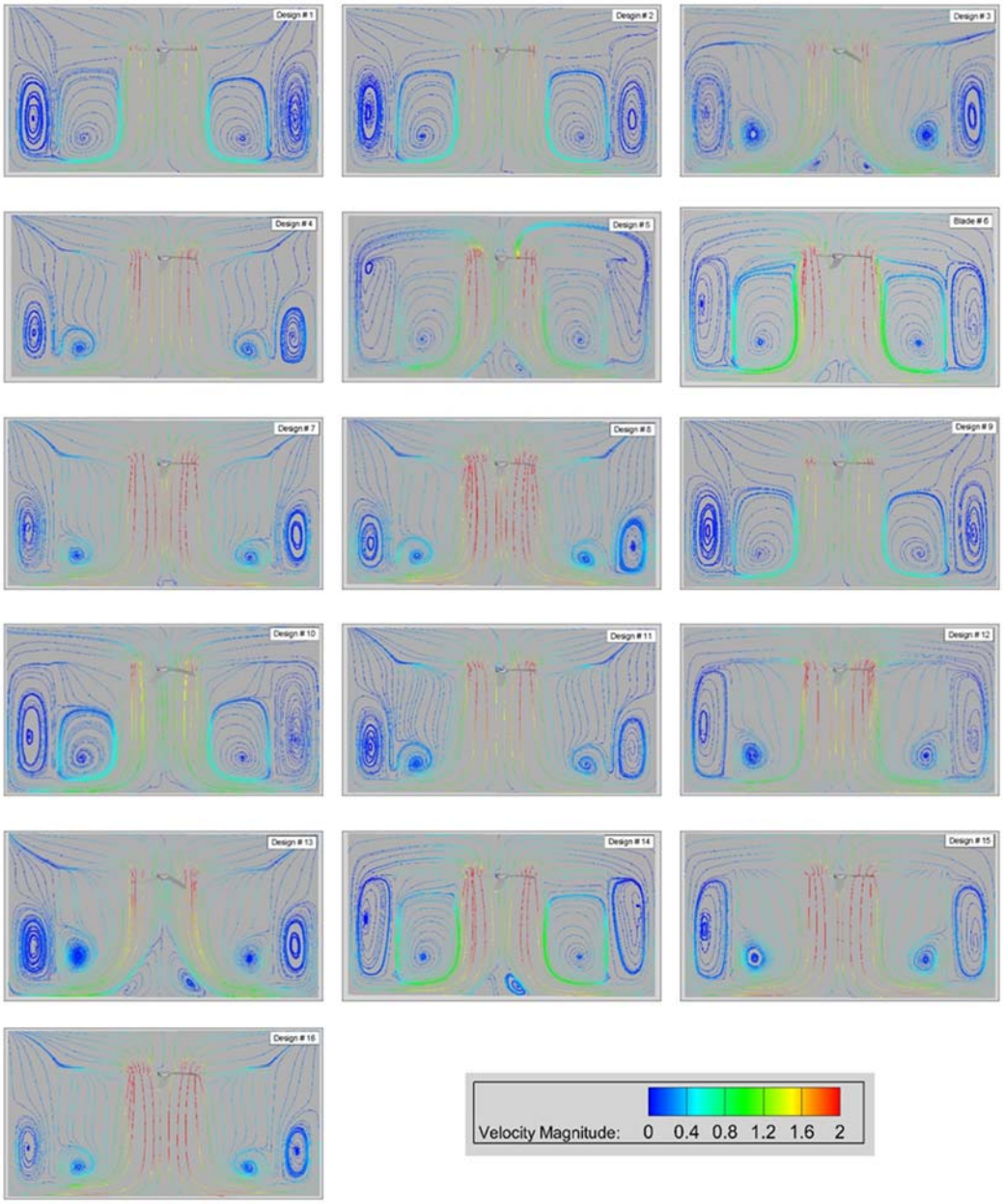

Fig. 7. Velocity contours at centre of room (slice taken at centre of x-plane

4.2 Optimization

Optimization is a major concern in today's life. Multi-objective optimization or, in other words, multi-criteria optimization, can be described as finding a satisfactory solution by satisfying constraints for an objective function. In this optimization problem, several objectives are optimized simultaneously. Sometimes objectives conflict; refining one response parameter affects another parameter. Therefore, a set of optimal solutions exists, and no single optimal solution is best. The control variables and objective function used in this research for optimization are defined as

$$J = [V_m, M_m, E_m, T_d] \quad (5)$$

$$J = -w_1.V_m - w_2.M_m + w_3.T_d - w_4.E_m \quad (6)$$

The four conflicting objectives simultaneously optimized in this study were volumetric flow increase (V_m), mass flow rate increase (M_m), energy efficiency increase (E_m), and torque decrease (T_d) with respect to the design variables (F, I, O and T), and the weighting was $w_1 = w_2 = w_3 = w_4 = 1$. Therefore, the multi-objective problem after applying the constraints can be described as

$$\begin{cases} Maximize & V_m, M_m, E_m\,(F,I,O,T) \\ Minimize & T_d \quad (F,I,O,T) \\ & Constraints \\ 0.05 \le F \le 0.15; & V_m approcah\ 185 \\ 6^0 \le I \le 12^0; & M_m\ approcah\ 3.7 \\ 6^0 \le O \le 12^0; & E_m\ approcah\ 180 \\ 0.058 \le T \le 0.117; & T_d \le 1.8 \end{cases}$$

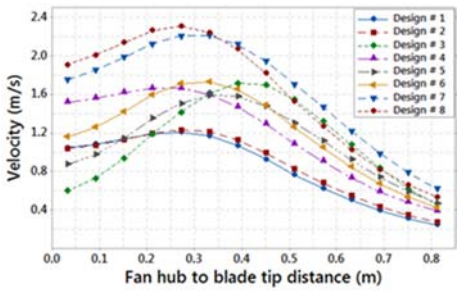

Fig. 8. Air velocity magnitude of design numbers 1 to 8

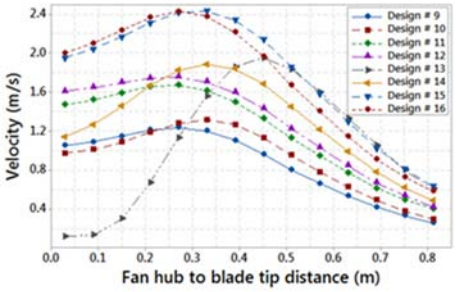

Fig. 9. Air velocity magnitude of design numbers 9 to 16

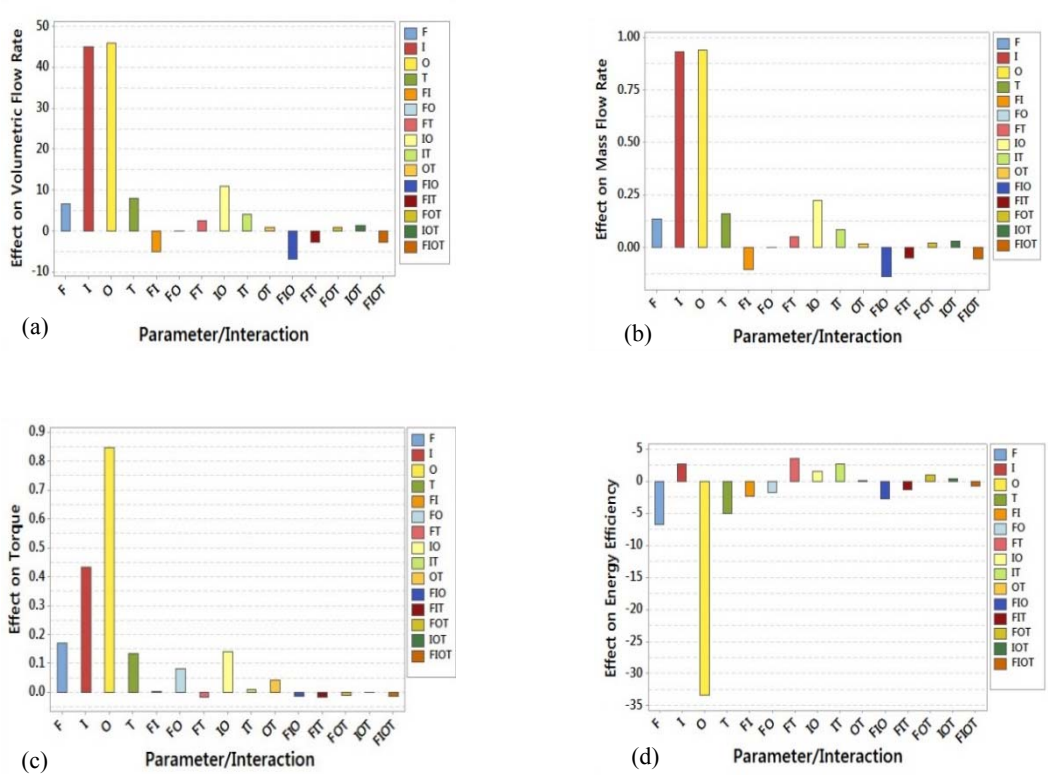

Fig. 10. Effect on geometric parameter and interactions of response parameters

Figure 12 depicts the attained optimum design points of the four objective functions and shows some interesting design facts. The first graph in Fig. 12 shows the composite desirability i.e. how all four response parameters were affected by changing the parameter F, which had a constant effect until the centre of graph and then decreased after that but with a very low slope. Similarly, as design variables I and O increased, the value of all other response parameters varied linearly, except for the case of geometric parameter O, which had a bell-shaped effect. The parameter F had a constant effect on the mass flow rate and volumetric flow rate, whereas it had a negative linear slope effect on energy efficiency and a positive slope effect on torque. Parameters I, O and T showed minimum values when the geometric parameter had a small value and increased when the geometric parameter increased. However, for energy efficiency, parameters O and T showed a decreasing trend but with different slopes.

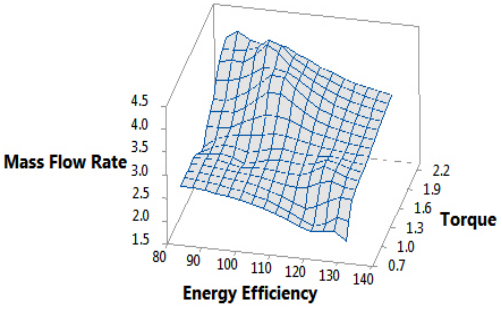

Fig. 11. Response surface of four-blade ceiling fan

The graphs of Fig. 12 clearly indicate the trade-off in the objective function from which a suitable design can be selected. All four responses at geometric optimum settings represented by the red line were chosen and the value is displayed above. Each response carried its own desirability, and the composite desirability was 0.97, demonstrating that the final design was very reliable for all performance indicators. The horizontal blue dotted lines show the level of response at these parameter settings. For validation purposes, the final design was computationally created in GAMBIT® and simulated in FLUENT®. A high degree of confidence was demonstrated between the test readings and the predicted values. Final results confirmed the successful application and implementation of the DOE and RSM for solving industrial problems related to the design and manufacturing of products. An optimized design was proposed which had maximum energy efficiency, volumetric flow rate, and mass flow rate and minimum torque.

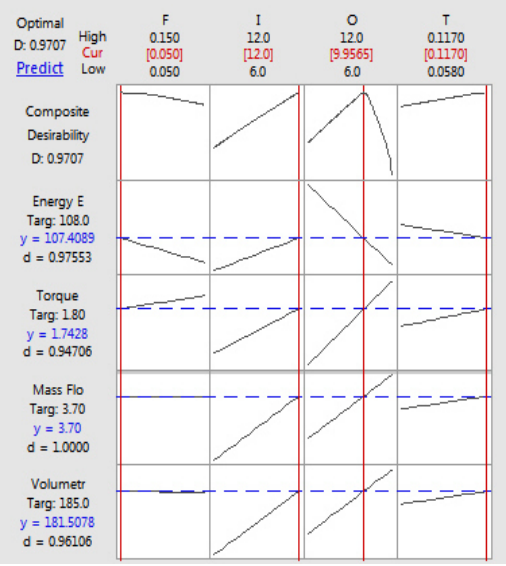

Fig. 12. Multi-objective optimum solution for 4 blade ceiling fan

5 CONCLUSION

A numerical study of airflow induced by a ceiling fan in a room was performed using the DOE technique, and the results depicted different flow regions in a room. Four geometric parameters were analyzed. In addition, a comparative study was conducted between the forward and reverse-sweep fan blades, and results revealed that the forward-sweep blade was more efficient and produced more volumetric flow rate and mass flow rate. Velocity magnitude was categorized in three different regimes. Two symmetric swirls were observed about the fan axis, and floor swirl was only observed for forward-sweep ceiling fan blades having a high-hump velocity profile. Linear ceiling fan blades produced no natural ventilation under the fan hub area, but a fan with a low-hump velocity profile produced more good natural ventilation. The results also revealed that the most influential geometric parameter was the outboard AOA. Further, fan blade design was optimized using the RSM which improved the performance of the ceiling fan; increased the energy efficiency, mass flow rate, and decreased torque.

ACKNOWLEDGEMENT

This work is supported by Basic Science Research Program through the National Research Foundation of Korea (NRF) funded by the Ministry of Education (NRF-2017R1D1A1B03032472).

REFERENCES

Adeeb. E., A. Maqsood, A. Mushtaq and Z. Hussain (2015). Shape Optimization of non-linear swept ceiling fan blades through RANS simulations and Response Surface Methods. *12th International Bhurban Conference on Applied Sciences and Technology*, IEEE.

Adeeb. E., A. Maqsood, A. Mushtaq (2015). Effect of number of blades on performance of ceiling fans. *4th International Conference on Advances in Mechanics Engineering*, IEEE.

Adeeb. E, A. Maqsood, A. Mushtaq and C.H. Sohn (2016). Parametric study and optimization of ceiling fan blades for improved aerodynamic performance. *Jouranl of Applied Fluid Mechanics* 9(6), 2905-2916.

Afaq, M. A., A. Maqsood, K. Parvez and A. Mushtaq (2014). Study on the design improvement of an indoor ceiling fan. *11th International Bhurban Conference on Applied Sciences and Technology*, IEEE.

Afaq, M. A., A. Maqsood, Butt. S. I., Tauqeer. T., and Hassan, A., (2017). Aerodynamic investigation and redesign of ceiling fan blades for enhanced energy efficieny. *Majeo International Journal of Science and Technology* 11(02), 97-114.

Ankur. J., Rochan. R. U., Samarth. C., Manish. S, and Sunil. K. (2004). Experimental Investigation of the Flow Field of a Ceiling Fan. *ASME 2004 Heat Transfer/Fluid Engineering Summer Conference*, Charlotte, North Carolinia, USA.

Makhoul, A., Ghali, K., and Ghaddar, N. (2013), Desk fan for the control of the convection flow around occupants using ceiling mounted personalized ventilation. *Buildings and environment* 59, 336-348.

Falahat, A. (2011). Numerical and Experimental Optimization of Flow Coefficient in Tubeaxial Fan. *International Journal of Multidisciplinary Sciences and Engineering* 2(5), 24-29.

Lin. S. C., and Hsieh. M. Y., (2014), An Integrated Numerical and Experimental Analysis for Enhancing the Performance of the Hidden Ceiling Fan. *Advances in Mechanical Engineering* 6.

Parker, D. S.,. Challahan, M. P. Sonne, J. K., Su, G. H., and Hibbs, B. D (2000). Development of a High Efficiency Ceiling Fan. *Florida Solar Center, 1679 Clearlake Road, Cocoa Florida 32922, USA.*

Bassiouny, R., and Nadar, S. K., (2011). Studying the Features of Air Flow Induced by a Room Ceiling-Fan. *Energy and Buildings,* 43(8), 1913-1918.

Schmidt, K. and Patterson, D. J., (2001) Performance result for a high efficiency tropical ceiling fan and comparisons with conventional fans. *Renewable Energy*, 22(1-3), 169-176.

Son. H. Ho, Rosario, L., and Rehman, M. (2009), Thermal comfort enhanchment by using a ceiling fan. *Applied Thermal Enginnering* 29(9), 1648-1656.

Spalart. P. R., and Allmaras. S. R., (1992). A One-Equation Turbulence Model for Aerodynamic Flows. *30th Aerospace Sciences Meeting and Exhibit. Seattle, Washington, United States*.